WILEY-VCH

DOI: 10.1002/ ((please add manuscript number))

Article type: Full Paper

Electrical and mechanical self-healing in high performance dielectric elastomer actuator materials

Yan Zhang[1], Christopher Ellingford[2], Runan Zhang[1], James Roscow[1], Margaret Hopkins[1], Patrick Keogh[1], Tony McNally[2], Chris Bowen[1], Chaoying Wan[2,]*

[1] Department of Mechanical Engineering, University of Bath, BA2 7AY, UK

[2] International Institute for Nanocomposites Manufacturing (IINM), WMG, University of Warwick, CV4 7AL, UK

Dr Yan Zhang, Dr Runan Zhang, Dr James Roscow, Dr Margaret Hopkins, Prof. Patrick Keogh, Prof. Chris Bowen,
Department of Mechanical Engineering, University of Bath, BA2 7AY, UK

Christopher Ellingford, Prof Tony McNally, Dr Chaoying Wan,
International Institute for Nanocomposites Manufacturing (IINM), WMG, University of Warwick, CV4 7AL, UK
Email: chaoying.wan@warwick.ac.uk

Keywords: electric breakdown and mechanical damage, self-healing, dielectric elastomer, breakdown recovery, actuation

Abstract

Dielectric elastomers are of interest for actuator applications due to their large actuation strain, high bandwidth, high energy density, and their flexible nature. If future dielectric elastomers are to be used reliably in applications that include soft robotics, medical devices, artificial muscles and electronic skins, there is a need to design devices that are tolerant to electrical and mechanical damage. In this paper, we provide the first report of self-healing of both electrical breakdown and mechanical damage in dielectric actuators using a thermoplastic methyl thioglycolate modified styrene-butadiene-styrene (MGSBS) elastomer. The self-healing functions are examined from the material to device level by detailed examination of the healing process, and characterisation of electrical properties and actuator response before and after healing. We demonstrate that after dielectric breakdown, the initial dielectric strength can be recovered by up to 67%, and after mechanical damage a 39% recovery can be achieved with no

degradation of the strain-voltage response of the actuators. The elastomer can also heal a combination of mechanical and electrical failures. This work provides a route to create robust and damage tolerant dielectric elastomers for soft robotic and other applications related to actuator and energy harvesting systems.

1. Introduction

Dielectric elastomers are of interest for actuator applications due to their large actuation strain, high bandwidth, high energy density, and their compliant and flexible nature [1]. They are also easy to manufacture since they consist simply of a low stiffness elastomer placed between two conductive electrodes [2]. When an electric field is applied across the elastomer, the attractive force between the oppositely charged electrodes reduces the elastomer thickness and increases its area to provide actuation. One disadvantage of this approach is that high electric fields are necessary to achieve significant shape change, leading to large operating voltages which can be in excess of 1 kV for elastomers less than 1 mm thick. Dielectric elastomers are also being used for energy harvesting, where the change in capacitance during deformation of the elastomer is used to increase the amount of stored electrical energy [3].

Due to the high operating electric field for both actuator and energy harvesting applications, the elastomer is susceptible to dielectric breakdown. The breakdown process is typically initiated at a defect within the elastomer that acts to concentrate the applied electric field. During breakdown the applied voltage is discharged through the elastomer between the two electrodes, leading to heating and vaporization to form a 'pin-hole' defect [4]. If dielectric elastomers are to be used reliably in applications such as soft robotics, medical devices, artificial muscles and electronic skins, there is a need in the future to design devices that are tolerant to such electrical damage.

One strategy to overcome electrically or mechanically induced damage is to develop elastomer devices with the ability to *self-repair* or *self-heal*. Dünki *et al*. [5] developed a dielectric silicone elastomer with a high permittivity and low Young's modulus for actuation. The actuation strain (s) is related to $s \propto (\varepsilon' \varepsilon_0 E_b^2)/Y$, where ε' is the relative permittivity, ε_0 is the permittivity of free space, Y is the Young's (elastic) modulus and E_b is the breakdown field of the material. Clearly for a high strain dielectric actuator, a combination of high permittivity and low elastic modulus is desirable, coupled with a high breakdown field to enable operation at high electric

fields[1]. The material developed by Dünki *et al*. exhibited a high permittivity ($\varepsilon' \sim 10.1$), low Young's modulus ($Y \sim 150$ kPa) and demonstrated an ability to *self-repair* after dielectric breakdown. The repair process during actuation was attributed to the burning of both the elastomer and electrode during breakdown events, which prevented the formation of conductive paths and electrical shorting. The process is similar to that used by Ahmed *et al*. [6] who used *self-clearing* to mitigate against early breakdown of dielectric elastomers at defect sites. This involved pre-clearing defects in a P(VDF-TrFE-CTFE) terpolymer prior to operation by applying an electric field to the material that eliminated defective regions by vaporizing the electrode and polymer, thereby electrically isolating the breakdown site. An improvement in breakdown strength of 18% was achieved compared to non-cleared material, and the loss of active area and capacitance during the pre-clearing process was less than 5%. Carbon based electrodes for dielectric actuators have also been developed that exhibit self-clearing for dielectric elastomer applications, which includes the use of graphite nano-platelets in a silicone matrix or carbon nanotubes [7] [8] [9] [10] [11].

As indicated by Hunt *et al.* [4], the process of self-clearing, or self-repair, leads to a progressive decrease in the performance of the dielectric elastomer device. This is different to the mechanism of *self-healing,* which we define here as the infilling and removal of any defects formed by damage [2]. Self-healing has a number of potential advantages. Firstly, unlike self-clearing, it can maintain device capacitance and device functionality [4]. Secondly, the healing process can lead to removal of breakdown defects that could potentially lead to mechanical failure, especially at the high strains and large operating cycles in actuator and energy harvesting applications. Finally, in addition to electrical damage, self-healing has the potential to recover any mechanical damage that the elastomer experiences in service or during processing; self-clearing is unable to provide such mechanical healing since it relies on electrical vaporization of the electrode around the defect site to electrically isolate any damage.

Work on true self-healing in dielectric elastomers has been limited to date. Hunt *et al.* [4] used a two-phase system based on a silicone sponge infilled with a silicone oil which would infill any breakdown defects, leading to an improved lifetime. Acome *et al.* [12] used a liquid dielectric to provide a healing mechanism, which was combined with a hydraulically amplified electro-static

[1] The parameter (ε'/Y) is also used since it relates to the strain per unit voltage and E_b defines the maximum applied voltage.

[2] 'Self-healing' is also used in the literature to describe self-clearing in capacitor applications, but for clarity 'self-healing' is used here to specifically describe the removal or defects.

actuator; liquid conductive electrodes have also been considered [13]. In an attempt to simplify device design, *solid* self-healing dielectric elastomers have been considered. Madsen *et al.* [14] created self-healing dielectric elastomers based on interpenetrating silicone and ionic networks with $\varepsilon' \sim 6.3$, $E_b \sim 56$ kV mm^{-1} and $Y \sim 400$ kPa. Visual evidence of self-healing around electrical breakdown 'pin-hole' sites was observed after thermal treatment, although the degree of recovery was not quantified. Li *et al.* [15] developed a poly(dimethylsiloxane) based material with $\varepsilon' \sim 6.4$, $E_b \sim 18.8$ kV mm^{-1} and $Y \sim 540$ kPa which could heal mechanical damage, but there was no detailed investigation on the healing of electrical breakdown.[15] Liu et al. reported a supramolecular elastomer that self-healed with $\varepsilon' \sim 64$ - 4126, $Y \sim 12$ - 400 kPa, and relatively low $E_b \sim 1.1$ - 9.5 kV mm^{-1} and demonstrated self-healing of mechanical damage in a dielectric elastomer, however, the high dielectric loss (tan δ) is a potential concern for device performance.[16] Finally, self-healing of mechanical and electrical damage was reported in hydrogen-bonded supramolecular polymer nanocomposites based on surface functionalized boron nitride nanosheets.[17]. The material exhibited healing after dielectric breakdown over five cycles; however, the combination of a low $\varepsilon' \sim 4$ and high $Y \sim 40$ MPa makes it undesirable for dielectric elastomer applications and the material was not tested in a device. He et al. [18] recently demonstrated healing of electrical damage in polypropylene, however the process required the addition of superparamagnetic iron oxide nanoparticles, rather than using intrinsic self-healing, and the use of filler particles can act to reduce electrical breakdown strength [19]. To date, there has been no quantitative demonstration of both electrical and mechanical healing in solid dielectric elastomers and the actuation properties of self-healed dielectric actuators have yet to be reported.

In this paper we provide the first report on self-healing of both electrical breakdown and mechanical damage in dielectric actuators using a thermoplastic methyl thioglycolate modified styrene-butadiene-styrene (MGSBS) dielectric elastomer. Only modest healing in the material was reported [20] when the site was left to naturally self-heal (6% recovery of initial breakdown strength) or pressure was applied without removal or cleaning of the pin-hole defect (15% recovery of initial breakdown strength). Self-healing performance of the material is examined in this work at both the microstructural and device levels by detailed examination of the healing process, understanding the healing mechanism of pin-holes, and by characterization and modelling of the electrical properties before and after self-healing. We also assess the actuation characteristics of self-healing dielectric actuators subjected to both electrical and mechanical damage, including a combination of mechanical and high dielectric strength. The material

exhibits high permittivity ($\varepsilon' > 10$), high dielectric strength ($E_b \sim 30$ kV mm^{-1}), low Young's modulus of 2.9 MPa and a large strain to failure of 600%. We demonstrate that after dielectric breakdown, the dielectric strength can be recovered by ~ 39% of initial strength after mechanical damage and by ~67% after electric breakdown. Furthermore, the displacement-voltage response of the actuator is unchanged after healing and infilling of breakdown defects. After being subjected to both mechanical and electrical damage, the elastomer can also retain its displacement-voltage characteristic when operating as an actuator.

2. Results and discussion

2.1 Observation of self-healed MGSBS elastomer after electrical breakdown

To evaluate the mechanism of healing of electrical damage, the elastomer was initially subjected to dielectric breakdown and the healing of the defect was examined by a combination of microscopy and electrical measurements at low and high electric fields. **Figure 1** shows a pin-hole defect formed during breakdown, and the corresponding scanning electron microscopy (SEM) and optical morphology of the elastomer after healing. To facilitate observation of the breakdown site and healing no electrode was used; similar pin-hole breakdown defects were formed when metallic electrodes were used (**Figure** S1). The pristine elastomer experienced electrical breakdown at a 9.5 kV voltage (and electric field of 32.8 kV mm^{-1}), as shown in **Figure 1**(A)-(1) which leads to the formation of a carbonized [21] pin-hole of ~ 90 μm in diameter, as shown in **Figure 1**(B). Both the upper and lower surfaces of the elastomer had carbon deposits produced near the defect, due to the reaction of the vaporized material with air during breakdown. In order to remove any carbon deposits nearby and within the pin-hole, the carbonized zone was penetrated through its thickness by a fine scale metallic needle probe, see **Figure 1**(A)-(2) and **Figure 1**(C). This led to the pin-hole defect exhibiting a more circular morphology and reduced the level of carbonized deposits to produce a smoother and cleaner inner surface for healing, as shown in **Figure 1**(D). The freshly formed new surface then healed due to the macromolecular interactions [20] between the MGSBS chains, as shown in **Figure 1**(E), where the healing site has some similarities with self-healing of polymers subjected to projectile punctures [22] [23]. The differences between healing of mechanical and electrical damage are discussed in more detail later in the paper. After healing the breakdown site, the surface of the elastomer exhibited a closed up and healed hole, **Figure 1**(E). This healing differs from many

reports on mechanically damaged self-healing elastomers where the damaged surface after cutting is flat and therefore becomes fully sealed[14] [15] [16] [17] [24] [25].

To gain a further insight into the healing of a pin-hole defect it was examined as a cross-section (side view), using a defect that was introduced via a needle probe, as in **Figure** S4(A). The site was then self-healed by applying pressure with fingers, where the damaged surface can be seen to self-heal in the central region with a partially closed morphology near the surface of both sides, as seen in **Figure** S5(B), which is in agreement with observation from the top view of the pin-hole breakdown defect in **Figure 1**(E). This approach has provided a simple alternative to cleaning of the damage site and accomplish self-healing of the elastomer at room temperature. This is in contrast to other self-healing techniques, which require a healing agent/catalyst [26], or more challenging healing conditions, such as high temperature (> 100 °C) [27], light [28], pH [29] or a long dwell time [30], to trigger the dynamic covalent bonding through thermal Diels–Alder chemistry, photochemical cycloaddition or disulphide interexchange reactions [31]. The electrical properties of the self-healed elastomer are now discussed.

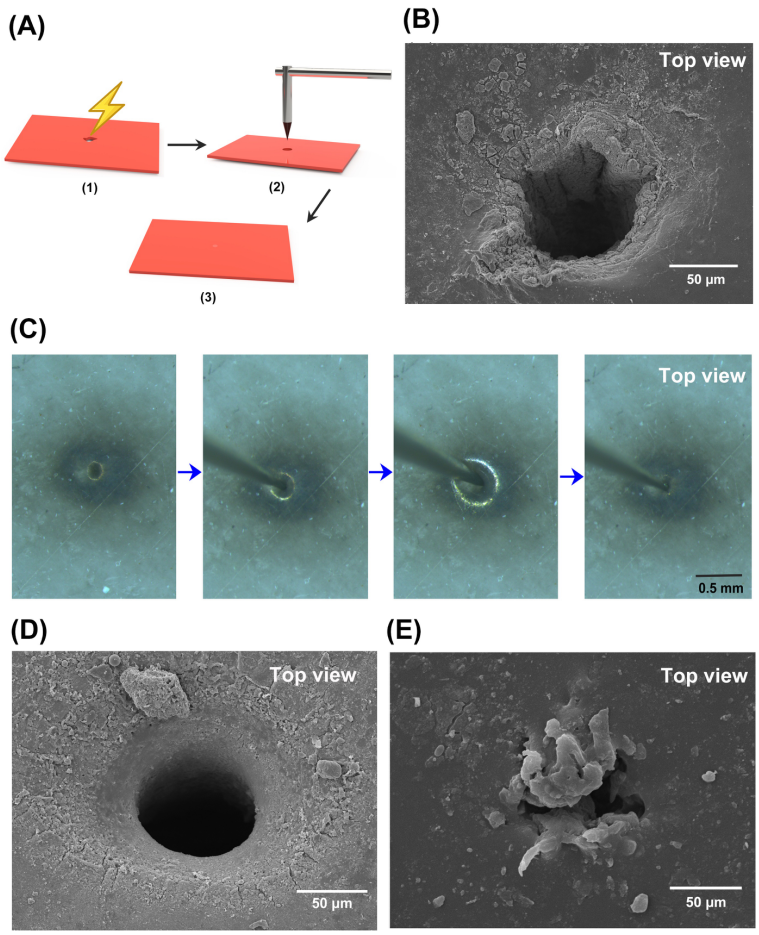

Figure 1. (A) Schematic of self-healing process for electrical breakdown MGSBS elastomer, (B) SEM images of the MGSSB surface after electrical breakdown, (C) optical images of the processing of the probe treatment on the elastomer surface, SEM images of the MGSSB surface (D) after probe treatment and (E) followed by application of pressure with fingers.

2.2 Electrical properties of self-healed MGSBS elastomer after electrical breakdown

Figure 2 shows the frequency dependent AC conductivity and dielectric properties of both the pristine MGSBS elastomer and self-healed elastomer after electric breakdown. It can be seen from Figure 2(A) to 2(C) that both types of elastomer exhibited a similar value and variation of AC conductivity, relative permittivity and phase angle in the frequency range of 1 Hz to 1 MHz. The limited change in properties indicates a promising healing effect via preclearing of the carbonized zone, thus reducing the possibility of forming an electrical short circuit due to the formation of a percolated conductive path of carbon through the pin-hole [20]. The AC conductivity of the elastomer in pristine and healed form was largely frequency independent at low frequencies below ~ 1 kHz, see **Figure 2**(A). However, at frequencies above 1 kHz, the AC conductivity became increasingly frequency dependent, as shown in **Figure 2**(A). Below this critical frequency of ~ 1 kHz, the low frequency conductivity plateau can be considered to be related to the DC conductivity of the material, where $\sigma_{DC} \sim 3\times10^{-10}$ S/m. The dispersive high-frequency region above 1 kHz follows Jonscher's universal law [32], where the AC conductivity $\sigma_{ac} \propto \omega^n$, where ω is the angular frequency and $n < 1$ is a fractional exponent. The low frequency conductivity plateau is due to the DC conductivity of the material, such as from ion migration in the MGSBS elastomer; this can be imagined as forming a series of resistors (R) with a frequency independent conductivity of R^{-1}. At frequencies above 1 kHz, ion vibration in the MGSBS elastomer leads to a more capacitive response [33] [34], as shown in **Figure 2**(A) and this can be imagined as a series of capacitors (C) with a frequency dependent conductivity ($\sim i\omega C$). The material exhibits a high relative permittivity in Figure 2(B) at low frequencies due to the resistive response of the MGSBS where an enhanced permittivity is often observed in a dielectric material exhibiting some conductivity [34]. At higher frequencies (10-10^5 Hz), the relative permittivity exhibited a frequency independent response, with a relative permittivity of $\varepsilon' \sim 11.8$ at 1 kHz, hence at higher frequencies the AC current passes through the capacitive regions since $\omega C > R^{-1}$. This behaviour can also be seen in the phase angle (θ) in Figure 2(C), where at low frequencies (below ~ 1 kHz) the response is more conductive and $\theta \rightarrow 0^\circ$ since $R^{-1} > \omega C$, while above 1 kHz the response is more capacitive with $\theta \rightarrow 90^\circ$ since $\omega C > R^{-1}$.

The characterization of conductivity, permittivity and phase angle was undertaken at a low electric field and an applied potential of V_{rms} = 0.1 V. However, for the evaluation of the electric performance as a dielectric actuator it is necessary to understand the material response and degree of healing when a high electric field is applied. The polarisation-field response of the pristine and healed MGSBS elastomers are shown in **Figure 2**(D) - 2(F). All samples exhibited an almost linear capacitive relationship with the applied voltage from 1 to 4 kV, corresponding to an electric field of 3.4 to 13.8 kV mm^{-1}, where 4 kV was the maximum voltage of the Radiant RT66B-HVi Ferroelectric Test system. This linear response originates from the dielectric response of the elastomer since the polarisation (and total charge, Q) is linearly related to applied field and voltage (V) by $Q = CV$. During the development of the carbonized zone preclearing process, two types of needles in terms of a solid probe (**Figure** S2, S3) and a larger hypodermic needle (**Figure** S4) were utilized to explore the healing efficiency. With the aid of the needle clearing at the electric breakdown site, both of the healed elastomers (**Figure 2**(E) and 2(F)) exhibited a similar polarisation-field behaviour to that of the pristine elastomer (**Figure 2**(D)). Moreover, the areas within the loop of the healed elastomers were slightly larger than the pristine elastomer at the same voltage, which we attribute to the slightly higher conductivity, as shown in **Figure 2**(A) [35]. The importance of the quality of the healing on the degree of recovered dielectric strength is demonstrated by the larger hypodermic needle experiencing breakdown at a relatively low applied voltage of 3.1 kV (**Figure 2**(E)), corresponding to a 36 % recovery of initial breakdown strength by healing. However, the elastomer healed with the finer needle probe was undamaged at 4 kV (**Figure 2**(F)), corresponding to a recovery of *at least* 47 % of the initial breakdown strength, and we will see later in the paper that healed actuators achieved 67% of initial breakdown strength prior to failure. This is larger than the modest healing reported by Wan *et al* [20] where damage was allowed to naturally self-heal (6% recovery of breakdown strength) or pressure was applied without cleaning of the pin-hole (15% recovery of breakdown strength).

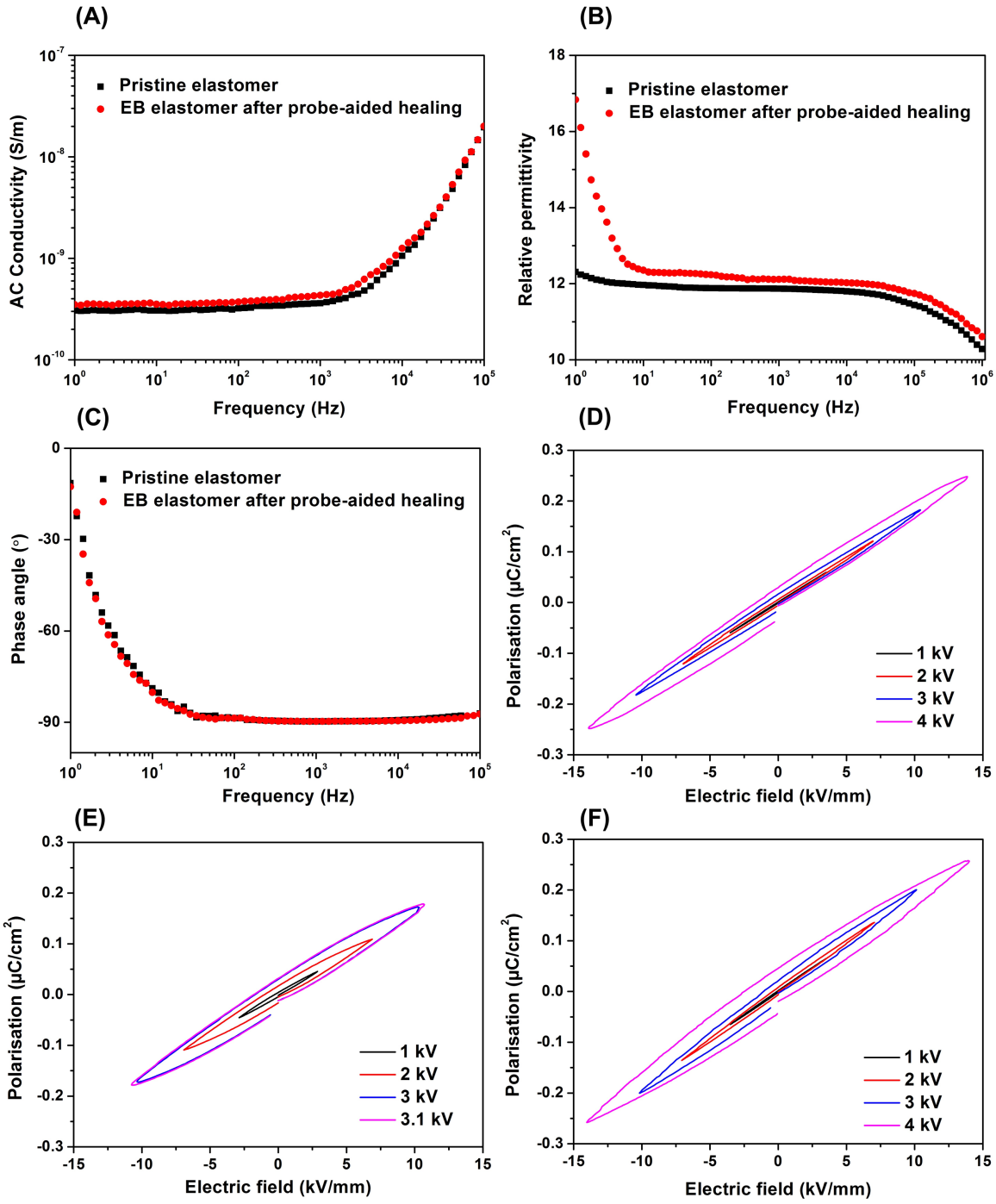

Figure 2. Electrical properties of MGSBS elastomers in pristine state and after self-healing from electric breakdown (EB): (A) AC conductivity, (B) relative permittivity, (C) phase angle and hysteresis loops of (D) pristine elastomer, self-healed elastomer whose carbonized zone was precleared via (E) larger hypodermic needle or (F) the finer solid needle probe using a micro-positioner.

2.3 Observation of self-healed MGSBS elastomer after mechanical damage

In addition to electrical healing, the response of the material after mechanical damage and its resulting electrical properties were also evaluated. **Figure 3** shows the healing process and corresponding SEM morphology of the MGSBS elastomer before and after mechanical damage. The pristine elastomer was cut fully through its thickness using a sharp and clean scalpel, as in **Figure 3**(A)-(1), and healed by applying a small load of 5N at ambient temperature for 5 min to ensure the damaged surfaces were in good contact and flattened in-plane. After healing, the cutting site (~ 25 mm in length) was fully closed and the healed site could be clearly observed when stretched normal to the cutting direction, as shown in **Figure 3**(A)-(2) and **Figure** S6(A). The healed MGSBS exhibited a 25% strength recovery with a strain of > 100%, as shown in **Figures** S6(B) and S6(C).

A top view of the surface morphology through the healing process is shown in Figure 3(B); images were taken directly after cutting and allowed to heal for a period of 5 min to 4 hours. The damage site shortly after cutting is shown in **Figure 3**(B-i), with the freshly cut surfaces initially attached together to achieve self-healing. During periodic inspection, the on-going healing process of the elastomer with initial partial bonding of the cut surfaces can be observed in **Figure 3**(B-ii); this process has been described by Kim and Wool [36], and proceeds by surface rearrangement, wetting, diffusion, and randomisation. The damaged site exhibited a significant improvement of the healing site after two hours due to continued healing, as shown in **Figure 3**(B-iii). Finally, an entirely closed fractured surface was found in **Figure 3**(C), which was in agreement with the observation from the cross-sectional image with the elastomer thickness of ~ 510 μm shown in **Figure 3**(D), which is common in fully healed elastomers after mechanical damage [14] [15] [16] [17] [37] [38].

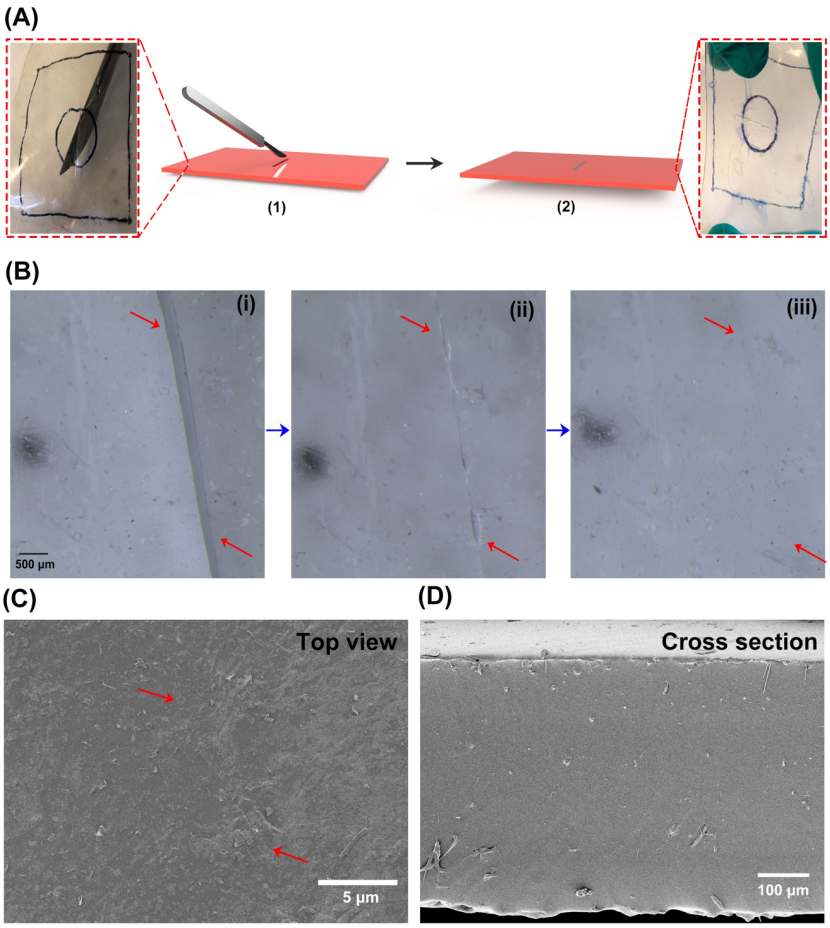

Figure 3. (A) Self-healing process for the mechanical damaged elastomer, (B) optical images of the MGSBS elastomer when (i) cut immediately, and healing after (ii) 5 min and (iii) 2 hrs. SEM images of the MGSSB after 4-hour healing from the (C) surface and (D) cross-section.

2.4 Electrical properties of self-healing MGSBS elastomer after mechanical damage

Figures 4(A) and 4(B) shows the AC conductivity and phase angle of the pristine MGSBS elastomer and self-healed after mechanical damage, respectively. As observed for the elastomers subjected to electrical breakdown in **Figure 2**, the mechanically healed elastomer exhibited a slightly higher AC conductivity and loss than the pristine polymer. In addition, since the damaged region (and resulting healing region) was larger than the pin-hole formed due to electrical breakdown, the conductivity increase was slightly larger. **Figures 4**(C) and 4(D) show the polarisation-field response of pristine and healed elastomer, respectively, and while the

pristine material experienced breakdown at 9 kV (17.6 kV mm^{-1}), the mechanically healed material experienced breakdown at over 3.4 kV (6.7 kV mm^{-1}), see **Figure 4**(D), corresponding to a healing of 38 % of the initial breakdown strength of the elastomer. The mechanically healed elastomer also exhibited a wider polarisation-field loop than the pristine elastomer and electrically damaged and healed material, shown in **Figure** S7, which is in agreement with the AC conductivity measurements (**Figures 2**A and 4A).

It is also of interest for dielectric actuator applications to understand the recovery of mechanical properties since the materials are subjected to mechanical strain. Self-healing of MGSBS resulted in a recovery of the mechanical properties to 116% elongation at break and a recovery to 0.8 MPa tensile strength; see **Figure** S6. This represents a recovery of 25% for the tensile strength and 21 % for the elongation at failure compared to pristine MGSBS, respectively. This indicates that self-healed MGSBS has the potential to be used for in healed actuator devices, which are typically subjected to a mechanical pre-strains of ~ 33%. [20]

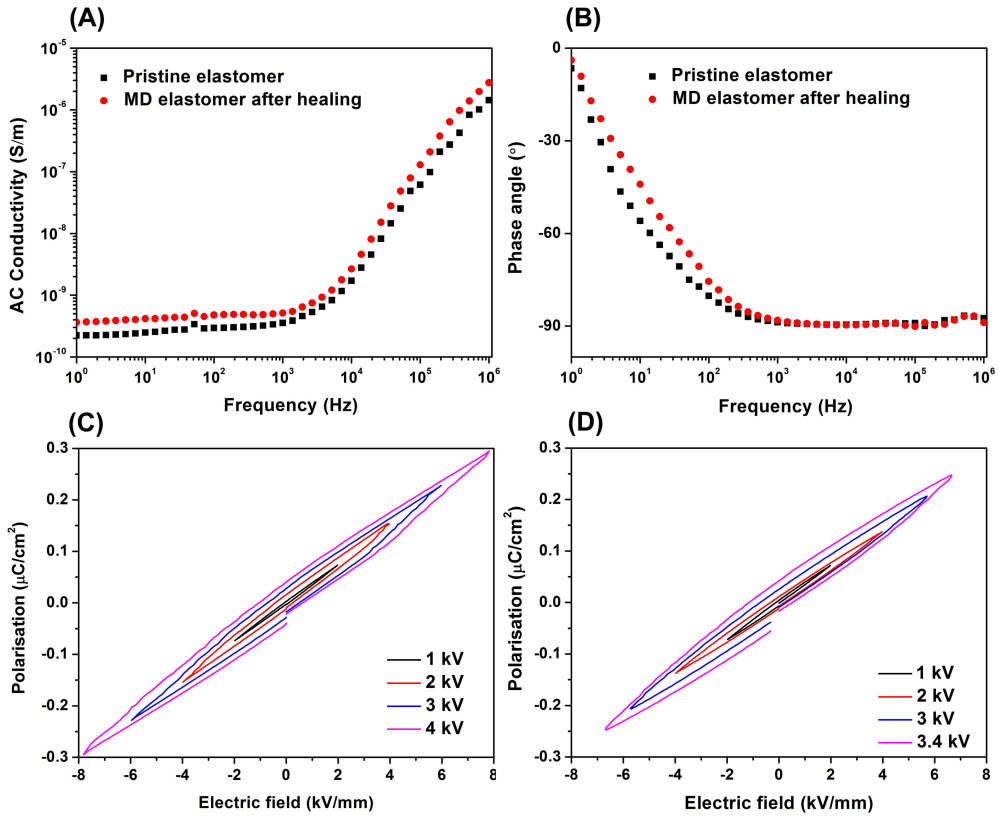

Figure 4. Electric properties of MGSBS elastomers in pristine state and after self-healing from mechanical damage (MD): (A) AC conductivity, (B) phase angle, and hysteresis loops of (C) pristine and (D) self-healed elastomers.

2.5 Self-healing mechanism of MGSBS elastomer

In contrast to many of the self-healing processes, there was no externally applied stimulus (catalyst, thermal, etc.) to promote the surface wetting and inter-diffusion of the new surfaces [39] [36] after either electrical breakdown or mechanical damage of the dielectric, other than a small mechanical pressure. The origin of the healing in this elastomer region may be ascribed to the intermolecular electrostatic interaction taking place between the methyl thioglycolate modified butadiene block and the styrene block of SBS [20]; this leads to a dynamic inter-chain interaction across the entire damage site which re-establishes bonding between the polymer chains due to the δ^+ proton adjacent to the ester interacting with the δ- aromatic centre of styrene. This process is shown schematically in **Figure 5**(A) which can be thought of as a series of 'lock and key' interchain junctions that lead to self-healing. The glass transition temperature (T_g = -22 °C [20]) of MGSBS is well below room temperature and so allows easy chain movement. A similar phenomenon for van der Waals interchain self-healing has been observed in poly(methyl methacrylate)/n-butyl acrylate block copolymers synthesized by multistep atom transfer radical polymerisation.[37]

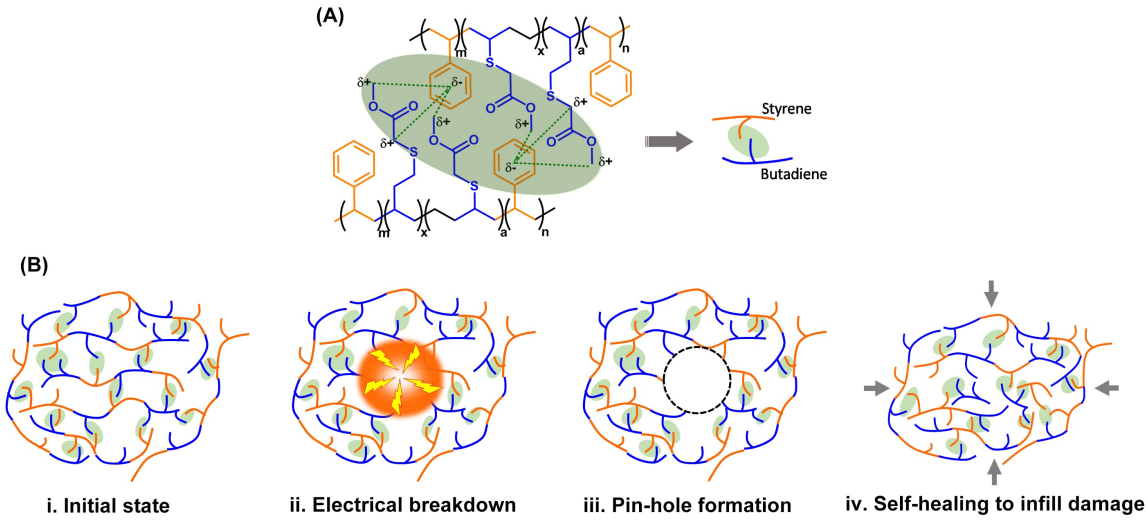

Figure 5. (A) Healing mechanism with the δ^+ proton adjacent to the ester interacting with the δ^- aromatic centre of styrene, (B) schematic of self-healing after electrical breakdown where (i) initial state, (ii) electrical breakdown leading to vaporization of polymer and (iii) formation of pin-hole, (iv) healing and infilling of pin-hole with application of pressure. Schematic is not to scale.

Self-healing after mechanical damage, such as cutting or fracture, has been described in detail in the literature[1, 40]. However, it is important to highlight that the nature of the damage induced by electrical breakdown is somewhat different which results in differences in the healing mechanism. Zakrevskii *et al.* [41] indicated that electrical breakdown is due to the presence of pores or low-density regions in the polymer that lead to ionisation, electron avalanche and ultimately the rapid progress of a conducting channel through the material. In contrast to mechanical damage, there is therefore vaporization and removal of material from the electrical breakdown site to create the pin-hole. In addition, there is unlikely to be any significant chain motion due to elastic or plastic deformation during the rapid breakdown process, as shown schematically in **Figure 5**(B)(i-iii). The application of a small pressure leads to healing and closure of the pin-hole, **Figure 5**(B)(iv), via the healing mechanism outlined in **Figure 5**A, where precleaning of the defect improves the degree of healing.

2.6 Modeling of self-healing MGSBS elastomer before and after breakdown

Since small defects are likely to remain after healing, for example surface defects as seen **Figure 1**(E) and S4, modeling was undertaken to understand the impact of surface defects and residual cavities post-healing on the electric field distribution within the elastomer and the resulting

progression of breakdown. This is particularly important since, as described above, the presence of any cavities or pores can lead to ionization and initiation of electrical breakdown [41].

The finite element modeling method consisted of creating an initial geometry for a healed material apart from the presence of small surface defects, see **Figure 6**(A), which are present after healing of the pin-hole, see **Figure 1**(E). An electrical load was applied to the model and the electric field in each element was assessed. When the local electric field within an element exceeded the breakdown strength of material, the permittivity of the material was changed from $\varepsilon' = 11.8$ (measured experimentally) to effectively an infinite value to represent the material becoming conductive [19] [42]. Once breakdown was initiated, the same electric field was applied, and the modeling sequence repeated, which led to progressive breakdown from the initiation sites. The upper images of **Figure 6** show the resulting propagation of breakdown (red areas) through the elastomer (blue), and shows that breakdown is initiated at the surface defects due to electric field concentrations subsequent breakdown of the polymer; the electric field distribution can be seen in the lower images of **Figure 6**. The effect of residual low permittivity cavities after healing is shown in **Figure S8**, whereby the field first concentrates in the low permittivity and low breakdown strength air phase ($\varepsilon' = 1$, $E_{b,air} = 3$ kV mm^{-1}), a condition of Gauss' law [43]. This results in localized dielectric breakdown of the air, which in turn causes the electric field to concentrate in the polymer phase. The breakdown defect then propagates through the structure until a complete conductive path between electrodes is present; see right image of **Figure 6**. The modeling results demonstrate that any low permittivity defects, cavities or pores which remain after the healing process can lead to high electric field concentrations, which ultimately act to initiate breakdown. Further modeling data is shown in **Figure S8** to demonstrate the impact of partial healing through the thickness, which may be the case during early stages of healing. This also indicates that voids or pores act to create electric field concentrations. These observations highlight the need to remove pores or any cavities after healing and is in good qualitative agreement with the improvement of the degree of healing as the healing methodology develops from natural healing (6%, [20]), application of pressure (15%, [20]), to using a large hypodermic needle (36%) and finally a fine solid needle (over 47%) to remove any carbon deposits and form a clean new surface for healing. The healing efficiency of materials subjected to electrical breakdown and mechanical damage will now be explored by integration of the material into an actuation device in the final section.

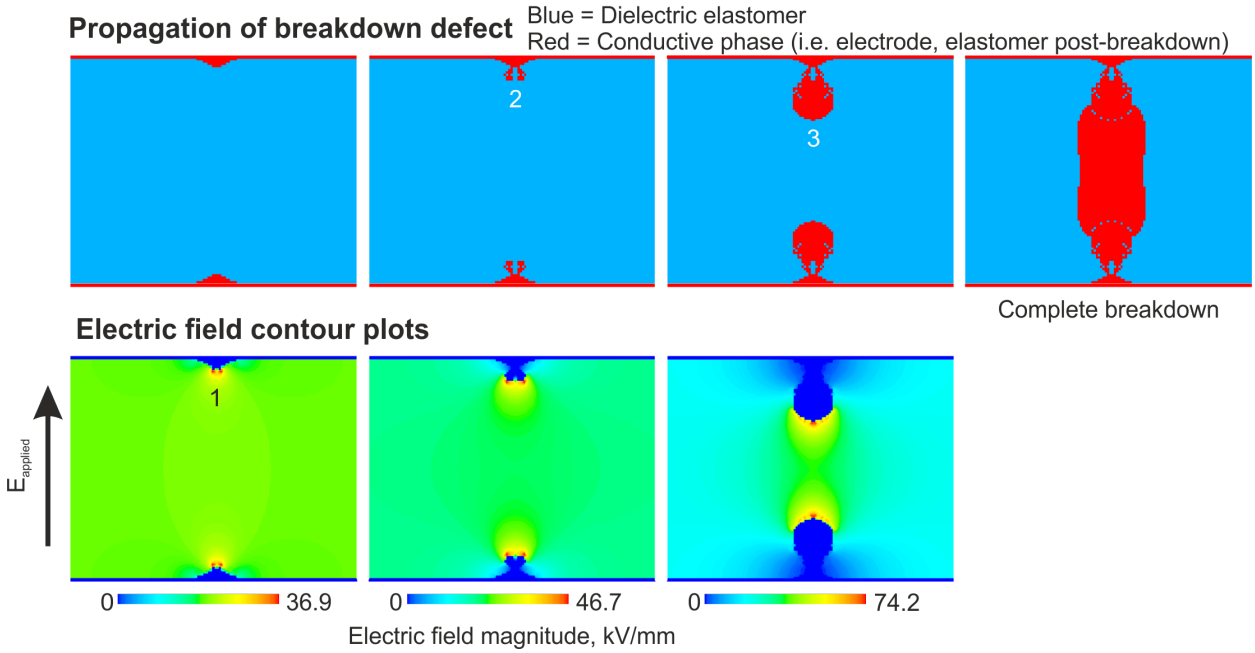

Figure 6. Finite element model showing the propagation of breakdown through a healed film due to a remnant surface defect, or an electrode defect. The surface defect leads to a field concentration in the healed elastomer in Region 1 that results in the initiation of a breakdown defect at Region 2. As the breakdown defect grows, the electric field is further concentrated in the dielectric elastomer phase, resulting in the defect propagating through the structure (2 → 3) and finally complete breakdown.

2.7 Dielectric actuator performance after electrical and mechanical healing

Figure 7 (A-D) shows the dielectric actuator devices manufactured from MGSBS after dielectric breakdown and mechanical healing under a 33% pre-strain after being clamped onto a rigid frame. A pre-strain is commonly employed in dielectric actuators to extract preferential actuation direction normal to that of the applied pre-strain direction [44], and it also leads to a reduced thickness and lower breakdown voltage. **Figure 7**(E) presents the corresponding radial actuation response of the pristine and healed actuator in response to the applied driving voltage. The pristine elastomer with a pre-strain exhibited dielectric breakdown as a voltage of 9 kV, corresponding to an electric field of 17.6 kV mm^{-1}. The breakdown site exhibited a circular shape with the diameter of ~ 1.5 mm, and this was much larger than the pin-hole (~90 μm) in the pre-strain free material in **Figure 1**; this is due to breakdown site being elastically deformed by the applied pre-strain. This is an additional reason for the need for self-healing in dielectric actuators and energy harvesters, rather than self-clearing, since these highly strained defects can act as initiation sites for further mechanical damage. It also highlights that in addition to infilling damaged areas with the elastomer to avoid electric field concentrations, as demonstrated by the

modelling, there is also a need to recover mechanical strength to avoid the healed defects from re-opening under the application of a strain during device operation.

After removal of the carbon grease electrode on the upper and lower sides of the elastomer, and cleaning of the carbonized area within the pin-hole via the needle probe to achieve self-healing (as in **Figure 1**), the same pre-strain was re-applied to the healed elastomer (**Figure 7**(B)). The actuation response under a high drive voltage was then re-evaluated, which experienced breakdown at a voltage of 6 kV, corresponding to an electric field of 11.8 kV mm^{-1}. This corresponded to a healing of the initial breakdown strength of 67 %, and the breakdown site was in the same region of the initial site, which is in good agreement with the modelling observation that any residual defects act to initiate breakdown due to electric field concentrations. A thinner healed MGSBS elastomer after electrical breakdown and healing is also illustrated in **Figure 9**, with the similar recovery of the initial breakdown strength ~60%. **Figure 7**(E) also shows that the strain-voltage response was also recovered with similar actuation strains being developed for the same applied voltage in the range of 0 - 5 kV for both the pristine and healed actuator.

The actuator was also subjected to mechanical damage by cutting and was then electroded with flexible carbon grease electrode after healing. The damaged region was 25 mm in length and traversed the whole electrode diameter of 15 mm, as shown in **Figure 7**(C). At an applied voltage of 3.5 kV (6.9 kV mm^{-1}), electrical breakdown occurred at a site with a diameter of ~0.5 mm in the presence of a pre-strain and breakdown initiated in the mechanically damaged and healing area. This corresponded to a degree of healing of 39 % of the initial breakdown strength and the actuator strain – voltage behaviour was the same for both the pristine and mechanically healed material from 0 to 3.5 kV. The electrical breakdown site in the healed region could be observed clearly after removing the electrode and being stretched, shown in **Figure 7**(D).

As a further demonstration of the healing properties of the actuator, the mechanically healed and electrically broken down device (**Figure 7**(D)) was self-healed again and re-evaluated as an actuator. After healing the electrical breakdown site in the mechanically damaged elastomer, the electrical strength recovery levels obtained were 86 % and 33 %, compared to the healed mechanical breakdown strength and the pristine breakdown strength, respectively. Based on the modelling observations in **Figure 6 and Figure S8**, the electric field concentrates in regions of low permittivity, e.g. air gaps, before concentrating in the elastomer as low permittivity sites begin to breakdown, and was thus responsible for the electrical breakdown at the same site in the healed material, resulting in electrical failure of the dielectric elastomer.

The majority of existing self-healing dielectric actuator research has focused on the elastomer materials, improvement of the healing conditions, and the corresponding healing performance of the elastomers after mechanical damage. The research to date is compared in **Table 1**, demonstrating that much of the work to date has focussed on mechanical healing. Since a high applied electric field is an inevitable condition to achieve dielectric actuation, it is an important factor that leads to electrical breakdown. Further work could focus on a combination of both infilling of the defect site with elastomer to remove electric field concentrations and improving healed mechanical strength due to the high strain and repeated cycles experienced by the actuator or self-healing devices.

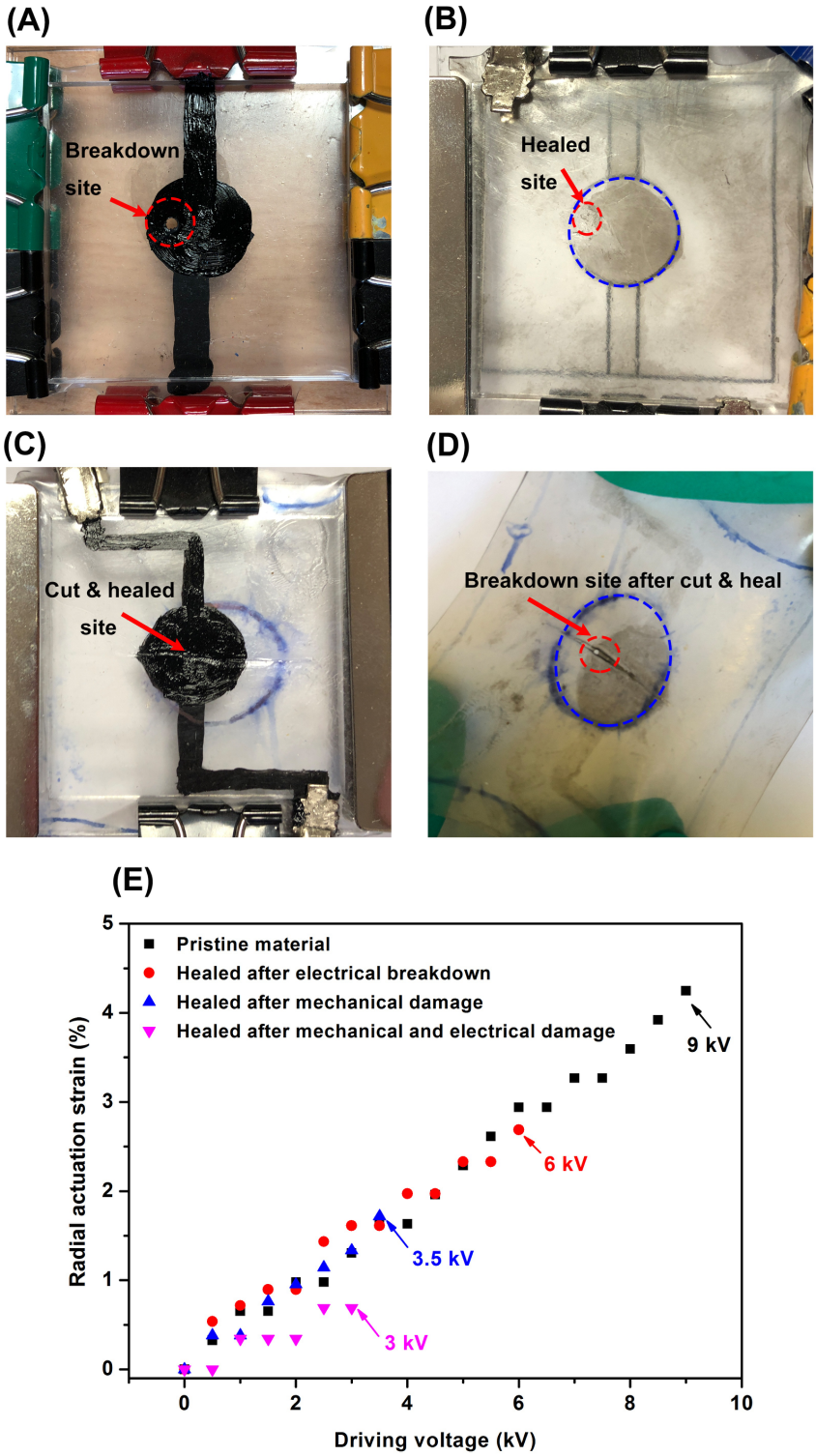

Figure 7. Actuator device with (A) pristine MGSBS elastomer after electrical breakdown with the thickness of 510 µm and (B) the correspondingly healed breakdown site before coating the flexible carbon grease on both sides for the actuation strain test. Actuator device (C) with self-healed MGSBS elastomer after mechanical damage via scalpel cutting and (D) the electrical breakdown site after application of a voltage of 9.25 kV (18.1 kV mm^{-1}). (E) Radial actuation strain of the pristine elastomer and healed elastomer after electrical, mechanical, or mechanical & electrical damage. All actuation measurements were conducted with a 33 % biaxial pre-strain on the elastomer.

Table 1 Comparisons of different self-healing dielectric elastomers after electrical breakdown or mechanical damage at room temperature

Dielectric elastomer	Relative permittivity, at 1 kHz	Tan δ, at 1 kHz	Breakdown strength, kV mm^{-1}	Young's modulus, MPa	Thickness, μm	Elongation at break	Mechanical healing	Electrical healing
Silicone rubbers[14]	~ 6.3	< 0.02	56	~ 0.4	100-200	387-982 %	√	×
Fe-2,6-pyridinedicarboxamide (Fe-Hpdca-PDM) [15]	~ 6.4	<0.025	18.8	~ 0.54	1000	1700 %	√	×
Nitrogen-coordinated boroxine-poly (propylene glycol)/poly (acrylic acid) [45]	-	-	-	2.7-112	~ 1000	182-659 %	√	×
Aniline tetramer functionalized supramolecular elastomer [16]	64-4126	~10	1.1-9.5	0.012-4	1000, 2000	350-1500 %	√	×
Functionalized boron nitride nanosheets-$CONH_2$ [17]	4	< 0.025	67.6 -232.6	1.5-135	1000	-	√	×
Poly(2-hydroxypropyl methacrylate)/poly(ethyleneimine) [24]	-	-	-	-	300	1000 %	√	×
Metal salts cross-linked PDMS[46]	2.9-3.5	-	-	0.9-1.2	~ 3.5	80-400 %	√	×
Disulfide-cross-linked polyurethane [25]	-	-	-	-	1000	~ 97 %	√	×
Urea-Formaldehyde - dicyclopentadiene [47]	-	-	-	-	-	-	×	√
MGSBS [20] & this work	11.4	~0.005	~ 30	2.9	290	569 %	√	√

[a] calculated data estimated from the relative figure reported in the reference.

3. Conclusions

A thermoplastic methyl thioglycolate modified styrene-butadiene-styrene (MGSBS) dielectric elastomer has been successfully used to provide the first demonstration of self-healing of both electrical breakdown and mechanical damage in dielectric actuators. It is shown that after dielectric breakdown, the dielectric strength can be recovered by up to 67% of initial strength, and after mechanical damage, 39% of the initial dielectric strength can be recovered. In addition, the displacement-voltage response of the actuator was not significantly changed after healing. The material was also shown to be able to heal a combination of mechanical and electrical failure. To maximize the degree of healing, the pin-hole defects were cleaned by being punctured with a needle of similar dimensions. This finding is in good agreement with modeling that demonstrates that low permittivity regions that have not fully healed can act as electric field concentrators to initiate breakdown. Future work could establish optimum elastomer and electrode chemistry and device geometry to achieve clean vaporization during breakdown and improve on this process. In this regard there is significant literature in the self-cleaning of polymer capacitors that can act to inform future research directions [48] [49] [50] [51]. This material

provides a route to create robust and damage tolerant dielectric elastomers for soft robotic and other applications related to future actuators and energy harvesting systems.

4. Experimental

4.1 Sample preparation

The synthesis of the polymer was reported in our previous work [20]. The styrene-butadiene-styrene block copolymer (SBS, Vector 8508A, Dexco) was dissolved in Tetrahydrofuran (THF, GPR Reactapur, 99.9%, VWR, UK). Then 2-dimethoxy-2-phenylacetophenone (DMPA, Sigma-Aldrich) and methyl thioglycolate (MG, Sigma-Aldrich) was added to the solution, followed by irradiating with UV light @ 365 nm by an OmniCure Series 2000 200 W UV lamp. After purification by precipitation in hexane (Sigma-Aldrich) and dried in a vacuum oven at 60 °C overnight, the MG modified SBS with 98.5% graft molar ratio was achieved and denoted as MGSBS.

4.2 Electrical breakdown and mechanical damage processes

To subject the MGSBS elastomer to electrical breakdown [20], an external DC voltage was applied using a high voltage power supply (module 15A24 from PPM^{TM}). In order to introduce mechanical damage, a scalpel was employed to mechanically cut through the thickness of the elastomer.

4.3 Self-healing

A binocular microscope with Leica camera (Plan APO 1.0x) was used to observe and locate the breakdown area in the elastomer subjected to electrical breakdown. A micropositioner (KRN-09S, J micro Technology, Inc) with a needle probe (ProbePoint^{TM} W20, J micro Technology, Inc) (**Figure S3**) was employed to punch the breakdown pin-hole in the elastomer, where a PDMS layer was used as a base to ensure the probe could travel through the full thickness of the elastomer (**Figure S2**). A video of the probe penetrating into the breakdown site is presented in Video 1, followed by application of a pressure with two fingers for ~ 5 min. For healing of elastomers subjected to mechanical damage, the new surfaces were placed together on a petri dish and covered by a ~ 0.5 kg load for ~ 5 min. As an initial assessment of healing of both electrical and mechanical induced damage, the material was manually strained by a small amount (~20%) to ensure that the defect site remained closed; for example Figure 3A(2). Both sides of the elastomers that were subjected to electrical breakdown and mechanical damage were then coated with silver paint as the electrodes for the following electrical measurements.

4.4 Electrical performance

The polarisation-electric field responses of the pristine MGSBS polymer, electrical breakdown and mechanical damage polymers after healing were tested using a Radiant RT66B-HVi Ferroelectric Test system with the hysteresis period of 10 ms. The AC conductivity, phase angle, and capacitance were carried out from 1 to 10^6 Hz using an impedance analyzer (Solartron 1260, Hampshire, UK) at room temperature.

4.5 Dielectric elastomer actuation (DEA)

For evaluation of dielectric actuation performance, all polymers were coated with carbon black grease (MG Chemicals) to form a circular electrode region of diameter 15 mm from the centre. A pre-strain of 33% in the polymer was realized in planar directions by being clamped onto a rigid frame. DC Voltages were increased from 0-10 kV to drive the actuation, with the material performance recorded by a camera to estimate the voltage-induced planar deformation. The DC voltages were also applied to evaluate the electrical breakdown strengths of the pristine and healed elastomers from electrical breakdown and/or mechanical damage, followed by the calculations of corresponding strength recovery compared to the initial breakdown strength of the pristine material.

Supporting Information

Supporting Information is available from the Wiley Online Library or from the author.

Acknowledgement

Dr Y. Zhang and Prof. C. R. Bowen would like to acknowledge the funding from the European Research Council under the European Union's Seventh Framework Programme (FP/2007–2013)/ERC Grant Agreement no. 320963 on Novel Energy Materials, Engineering Science and Integrated Systems (NEMESIS). The Leverhulme Trust is acknowledged by Prof. C. R. Bowen with the project no. RPG-2018-290. Mr C. Ellingford thanks EPSRC and Jaguar Land Rover (UK) for funding this PhD studentship.

Received: ((will be filled in by the editorial staff))
Revised: ((will be filled in by the editorial staff))
Published online: ((will be filled in by the editorial staff))

References

[1] D. Y. Wu, S. Meure, D. Solomon, *Progress in Polymer Science* **2008**, 33, 479.
[2] R. A. Bilodeau, R. K. Kramer, *Frontiers in Robotics and AI* **2017**, 4.
[3] C. Graf, Hitzbleck, J., Feller, T., Clauberg, K., Wagner, J., Krause, J., & Maas, J. , *Journal of Intelligent Material Systems and Structures* **2013**, 25, 951.
[4] S. Hunt, T. G. McKay, I. A. Anderson, *Applied Physics Letters* **2014**, 104, 113701.
[5] S. J. Dünki, Y. S. Ko, F. A. Nüesch, D. M. Opris, *Advanced Functional Materials* **2015**, 25, 2467.
[6] A. Saad, O. Zoubeida, T. L. Michael, *Smart Materials and Structures* **2017**, 26, 105024.
[7] S. Michel, B. T. T. Chu, S. Grimm, F. A. Nüesch, A. Borgschulte, D. M. Opris, *Journal of Materials Chemistry* **2012**, 22, 20736.
[8] H. Stoyanov, P. Brochu, X. Niu, C. Lai, S. Yun, Q. Pei, *RSC Advances* **2013**, 3, 2272.
[9] W. Yuan, T. Lam, J. Biggs, L. Hu, Z. Yu, S. Ha, D. Xi, M. K. Senesky, G. Grüner, Q. Pei, presented at SPIE Smart Structures and Materials + Nondestructive Evaluation and Health Monitoring **2007**.
[10] W. Yuan, L. B. Hu, Z. B. Yu, T. Lam, J. Biggs, S. M. Ha, D. J. Xi, B. Chen, M. K. Senesky, G. Grüner, Q. Pei, *Advanced Materials* **2008**, 20, 621.
[11] W. Yuan, H. Li, P. Brochu, X. Niu, Q. Pei, *International Journal of Smart and Nano Materials* **2010**, 1, 40.
[12] E. Acome, S. K. Mitchell, T. G. Morrissey, M. B. Emmett, C. Benjamin, M. King, M. Radakovitz, C. Keplinger, *Science* **2018**, 359, 61.
[13] Y. Liu, M. Gao, S. Mei, Y. Han, J. Liu, *Applied Physics Letters* **2013**, 103, 064101.
[14] F. B. Madsen, L. Yu, A. L. Skov, *ACS Macro Letters* **2016**, 5, 1196.
[15] C.-H. Li, C. Wang, C. Keplinger, J.-L. Zuo, L. Jin, Y. Sun, P. Zheng, Y. Cao, F. Lissel, C. Linder, X.-Z. You, Z. Bao, *Nature Chemistry* **2016**, 8, 618.
[16] L. Liu, S. Yan, L. Zhang, *Macromolecular Rapid Communications* **2018**, 39, 1800349.
[17] L. Xing, Q. Li, G. Zhang, X. Zhang, F. Liu, L. Liu, Y. Huang, Q. Wang, *Advanced Functional Materials* **2016**, 26, 3524.
[18] Y. Yang, J. He, Q. Li, L. Gao, J. Hu, R. Zeng, J. Qin, S. X. Wang, Q. Wang, *Nature Nanotechnology* **2018**, DOI: 10.1038/s41565-018-0327-4.
[19] C. R. B. J. I. Roscow, and D. P. Almond, *ACS Energy Letters* **2017**, 2, 2264.
[20] C. Ellingford, R. Zhang, A. M. Wemyss, C. Bowen, T. McNally, Ł. Figiel, C. Wan, *ACS Applied Materials & Interfaces* **2018**, 10, 38438.
[21] M. G. J. J. C. B. F. Carpi, *Proc. SPIE 10163, Electroactive Polymer Actuators and Devices (EAPAD) 2017, 101632B (17 April 2017); doi: 10.1117/12.2258617* **2017**.
[22] S. J. Kalista, T. C. Ward, Z. Oyetunji, *Mechanics of Advanced Materials and Structures* **2007**, 14, 391.
[23] R. Fall, *Master* Virginia Polytechnic Institute and State University, **2001**.
[24] W. Huang, K. Besar, Y. Zhang, S. Yang, G. Wiedman, Y. Liu, W. Guo, J. Song, K. Hemker, K. Hristova, I. J. Kymissis, H. E. Katz, *Advanced Functional Materials* **2015**, 25, 3745.
[25] T.-P. Huynh, H. Haick, *Advanced Materials* **2016**, 28, 138.
[26] T. S. Coope, D. F. Wass, R. S. Trask, I. P. Bond, *Macromolecular Materials and Engineering* **2014**, 299, 208.
[27] X. Chen, M. A. Dam, K. Ono, A. Mal, H. Shen, S. R. Nutt, K. Sheran, F. Wudl, *Science* **2002**, 295, 1698.
[28] Y. Amamoto, H. Otsuka, A. Takahara, K. Matyjaszewski, *Advanced Materials* **2012**, 24, 3975.
[29] Y. Zhang, B. Yang, X. Zhang, L. Xu, L. Tao, S. Li, Y. Wei, *Chemical Communications* **2012**, 48, 9305.
[30] J. D. Rule, E. N. Brown, N. R. Sottos, S. R. White, J. S. Moore, *Advanced Materials* **2005**, 17, 205.
[31] F. Herbst, S. Seiffert, W. H. Binder, *Polymer Chemistry* **2012**, 3, 3084.
[32] A. K. Jonscher, *Nature* **1977**, 267, 673.
[33] C. R. Bowen, S. Buschhorn, V. Adamaki, *Pure & Applied Chemistr* **2014**, 86, 765.
[34] D. P. Almond, C. R. Bowen, *The Journal of Physical Chemistry Letters* **2015**, 6, 1736.
[35] J. F. Scott, *Journal of Physics: Condensed Matter* **2008**, 20, 021001.
[36] Y. H. Kim, R. P. Wool, *Macromolecules* **1983**, 16, 1115.

[37] M. W. Urban, D. Davydovich, Y. Yang, T. Demir, Y. Zhang, L. Casabianca, *Science* **2018**, 362, 220.
[38] E. B. Murphy, E. Bolanos, C. Schaffner-Hamann, F. Wudl, S. R. Nutt, M. L. Auad, *Macromolecules* **2008**, 41, 5203.
[39] R. P. Wool, K. M. O'Connor, *Journal of Applied Physics* **1981**, 52, 5953.
[40] Y. Yang, M. W. Urban, *Chemical Society Reviews* **2013**, 42, 7446.
[41] V. A. Zakrevskii, N. T. Sudar, A. Zaopo, Y. A. Dubitsky, *Journal of Applied Physics* **2003**, 93, 2135.
[42] A. Konrad, M. Graovac, *IEEE Transactions on Magnetics* **1996**, 32, 4329.
[43] J. I. Roscow, R. W. C. Lewis, J. Taylor, C. R. Bowen, *Acta Materialia* **2017**, 128, 207.
[44] R. Pelrine, R. Kornbluh, Q. Pei, J. Joseph, *Science* **2000**, 287, 836.
[45] C. B. Y. J. J. H. Z. X. L. J. Sun, *Advanced Functional Materials* **2018**, 28, 1800560.
[46] Y.-L. Rao, A. Chortos, R. Pfattner, F. Lissel, Y.-C. Chiu, V. Feig, J. Xu, T. Kurosawa, X. Gu, C. Wang, M. He, J. W. Chung, Z. Bao, *Journal of the American Chemical Society* **2016**, 138, 6020.
[47] C. Lesaint, V. Risinggård, J. Hølto, H. H. Sæternes, H. Ø, S. Hvidsten, W. R. Glomm, presented at 2014 IEEE Electrical Insulation Conference (EIC), 8-11 June 2014, **2014**.
[48] N. Klein, presented at 1965 International Electron Devices Meeting, 20-22 Oct. 1965, **1965**.
[49] C. W. Reed, S. W. Cichanowskil, *IEEE Transactions on Dielectrics and Electrical Insulation* **1994**, 1, 904.
[50] J. Kammermaier, *IEEE Transactions on Electrical Insulation* **1987**, EI-22, 145.
[51] J. Kammermaier, G. Rittmayer, S. Birkle, *Journal of Applied Physics* **1989**, 66, 1594.